CCFE
CULHAM CENTRE FOR FUSION ENERGY

UK Atomic Energy Authority

UKAEA-CCFE-CP(23)14

S.F. Smith, S.J.P. Pamela, A. Fil, M. Hölzl, G.T.A. Huijsmans, A. Kirk, D. Moulton, O. Myatra, A.J. Thornton, H.R. Wilson

ELM BURN-THROUGH SIMULATIONS FOR MAST-U SUPER-X PLASMAS

ELM BURN-THROUGH SIMULATIONS FOR MAST-U SUPER-X PLASMAS

S.F. Smith, S.J.P. Pamela, A. Fil, M. Hölzl, G.T.A. Huijsmans, A. Kirk, D. Moulton, O. Myatra, A.J. Thornton, H.R. Wilson

This paper has been submitted to
28th IAEA Fusion Energy Conference, Nice, France, 10-15th May 2021

ELM BURN-THROUGH SIMULATIONS FOR MAST-U SUPER-X PLASMAS

S.F. SMITH, S.J.P. Pamela, A. Fil, A. Kirk, D. Moulton, O. Myatra, A.J. Thornton
CCFE-UKAEA Culham Science Centre
Abingdon, United Kingdom

M. Hölzl
Max Planck Institute for Plasma Physics
Garching .b M., Germany

G.T.A. Huijsmans
CEA, IRFM
Saint-Paul-Lea-Durance, France

H.R. Wilson
York Plasma Institute
York, United Kingdom

Email: siobhan.smith@ukaea.uk

Abstract

The high heat fluxes to the divertor during edge localised mode (ELM) instabilities have to be reduced for a sustainable future tokamak reactor. A solution to reduce the heat fluxes could be the Super-X divertor, this divertor configuration will be tested on MAST-U. ELM simulations for MAST-U Super-X tokamak plasmas have been obtained, using JOREK. Questions of ELM burn-through can only be answered with confidence when MAST-U starts operation, but until then simulations can provide useful guidance. A detached divertor MAST-U case is used as a starting point for the ELM burn-through simulations. The plasma burns through the neutrals front during the ELM causing the divertor plasma to re-attach. After the ELM crash a transition back to detachment is indicated, where the recovery to pre-ELM divertor conditions occurs in a few milliseconds, when the neutral pressure is high in the divertor. Recovery times are shorter than the type I inter-ELM phase in previous MAST experiments. The peak ELM energy fluence obtained after the ELM burn-through is 0.82 kJ/m^2, which is significantly lower than that predicted from the empirical scaling of the ELM energy fluence - indicating promising results for future MAST-U operations.

1. INTRODUCTION

For a successful future fusion power plant, different modes of operation need to be identified and explored. When finding the optimum operating regime a balance, between high plasma confinement and an operational mode that does not cause damage to the machine, is required. High confinement mode (H-mode) [1] is the favoured operation regime for tokamaks, due to the increased core plasma pressure, in comparison to other operating regimes. However, as the plasma edge pressure gradient and current density reach critical limits, explosive behaviour is observed; these magneto-hydrodynamic (MHD) instabilities are called edge localised modes (ELMs) and are quasi-periodic [2]. Type I ELMy H-mode regimes produce high confinement plasmas but are predicted to damage plasma facing machine components in future devices. Therefore, it is of importance to explore other operational regimes. In order to reduce ELM heat fluxes, various control mechanisms are being explored to obtain suppression or mitigation including RMPs, pellets and kicks [3–5]. Alternative exhaust geometries are also being researched to reduce heat fluxes incident on divertor targets.

The MAST-U tokamak will test a new Super-X divertor configuration [6], it will be investigated to determine whether it will be a suitable alternative exhaust system for future devices. Additional poloidal field coils have been installed, to direct the plasma into the Super-X divertor(s) and to allow control of the strike point radius length (R_s). At larger R_s the contact area of the plasma increases, which decreases the target heat flux. In addition, flux expansion in the chamber is also possible increasing the neutral interaction volume before the plasma reaches the targets [7]. The divertor is closed with a baffle, this design allows for retention of neutrals [7]. The baffle is important for attaining detachment whilst keeping impurities low in the core plasma. The detachment process allows for an increase in the radiated energy of the plasma before it reaches the targets. Operating in a (partially) detached regime will be beneficial, especially in future tokamaks such as ITER [8]. Detachment can be achieved by increasing the upstream plasma density or by increasing radiative losses through an impurity seeding ramp, which leads to an increase in recycling in the divertor and an increase in neutral density at the targets, where atomic processes play a key role. Plasma detachment has been predicted in the MAST-U Super-X for L-mode [9] and H-mode [10] plasmas but behaviour during ELMy H-mode is unknown. Here, simulations are used to address this by investigating the extent of ELM burn-through. We present first simulations of ELMs in MAST-U, in advance of its operation. The JOREK code [11 , 12, 13] is used for the simulations, JOREK is

a 3D non-linear MHD code, which is being actively validated against current experiments, including studies of MAST [14].

Section 2. gives an overview of the JOREK model used for the simulations. Section 3. details the detached divertor scenario in JOREK and compares this with a MAST-U Super-X SOLPS case. In section 4. the ELM burn-through simulations are shown, with energy fluence comparisons to other divertor scenarios in MAST-U. The ELM losses, filaments, burn-through and recovery are also discussed. A summary is given in section 5. with details of what further work could be performed.

2. JOREK AND MAST-U EQUILIBRIUM

A reduced two-temperature fluid model with diffusive neutrals has been used for the simulations. It is implemented in JOREK, where the model equations and full details are given in [15]. The neutrals model has been used previously for MGI and disruption simulations in JOREK [16] and is adapted here for divertor recycling, due to the increased plasma-neutral interactions in the Super-X, where plasma incident on the wall and targets is reflected away as diffusive neutrals. The flux of plasma at the divertor targets increases target neutral density and an ionisation front is established. This simple fluid neutrals model only includes deuterium atoms, the ionisation and recombination processes along with radiative processes with energy losses through line and bremsstrahlung radiation. The radiation rate coefficients are computed using ADAS data [17]. The simulations appear to produce an ionisation front which is detached from the target, despite the detailed atomic processes required for advanced detachment studies, which are not included in the model, such as charge exchange, molecular dissociation and impurities. This detached state is sufficient as an initial condition for first studies of ELM burn-through, but missing physics could be included in future work, including extra species and atomic processes. A simple model has initially been used, as the multiple toroidal mode number ELM simulation presented here already requires approximately three million core hours to run on the MARCONI Cineca supercomputer, and the computational time will further increase by incorporating additional physics.

The simulations use temperature dependant Spitzer resistivity and viscosity and Braginskii parallel thermal conductivities. Hyper-diffusive coefficients are used for numerical stability but do not interfere with the physics. Profiles are used to represent the H-mode transport barrier; the perpendicular diffusivity for density and temperature are given as radial profiles, which dip in the pedestal region. The fluid neutrals are described with a diffusive coefficient, parameter scans of this coefficient have been performed and are given in [18]. An ideal wall boundary condition is applied. Where the boundary of the computational domain coincides with a flux surface, Dirichlet boundary conditions are applied for density/temperature/velocity. For boundaries with which the flux is incident, such as the targets, there are free outflow boundary conditions for the density and temperature, in the model without neutrals. In the neutrals model, the density is reflected back as diffusive neutrals, where a reflective coefficient is defined, close to 100%. This parameter has been scanned and the results are given in [15]. Bohm and sheath boundary conditions are implemented for the parallel velocity where the magnetic flux is not parallel to the boundary. This is to represent the sheath at the boundary, which forces the parallel velocity to equal the sound speed.

The MAST-U equilibrium is generated with an extended outer leg, using the Fiesta code [19 , 20]. B_T = 0.64 T, the plasma current is 1 MA, q_{axis} = 1.1, q_{95} = 7.9 and the central density and sum of the electron and ion temperatures are 0.52×10^{20} m^{-3} and 1.8 keV, respectively. The temperature and density profiles are based on MAST pulse #24763 and are unstable to the peeling-ballooning modes that drive ELMs. The mid-plane profiles for the normalised pressure, normalised current density, q, density and temperature used in the MAST-U simulations are given in [15]. As MAST plasmas have a high rotation, a parallel velocity profile is included in the simulations. E × B background flows are also included but diamagnetic drifts are left out of the simulations. The Grad-Shafranov equation is solved again within JOREK for the magnetic flux and a grid is built. To account for the bootstrap current, an additional perturbation to the parallel current at the plasma edge is implemented, in the future a more realistic current profile can be obtained using the wide set of diagnostics available on MAST-U. The JOREK grid is a set of 2D Bezier finite elements in poloidal plane (R,Z) and is flux aligned to capture fast parallel transport, until just a few cm outside the separatrix. The grid is then extend to the MAST-U wall [21], such that the wall boundary conditions are represented correctly. A Fourier decomposition is used in the toroidal direction, due to the periodicity, allowing for investigations into single toroidal mode numbers with the benefit of reduced computational time.

Once the equilibrium and MAST-U grid have been obtained, the simulation is first run with equilibrium flows only (n = 0). Firstly, this allows the Bohm boundary conditions to diffuse from the boundary and secondly it allows the recycling of neutrals from the wall. For the ELM study, a quasi-steady state first has to be reached then a perturbation can be introduced, in the form of single/multiple toroidal mode numbers, to seed the ELM. The initial perturbation is much smaller than the equilibrium fields, typically at the level of numerical noise. This initial perturbation only increases if the equilibrium is unstable. When the non-linear phase of the simulation is reached an ELM crash occurs and a saturation phase follows.

3. OBTAINING A DETACHED DIVERTOR

Before the ELM simulations are performed, with the JOREK diffusive neutrals two temperature model, it is first important to demonstrate detachment, or to at least obtain a high neutral density in the divertor with the JOREK neutrals model. A Super-X MAST case has been used, with expanded divertor flux, close to a case given in [10], to allow for a comparison to SOLPS [22]. A scan in the upstream density is performed, five test cases are each run for 30 ms, until a saturated state is reached to allow neutral density to build up in the divertor. The cases have different upstream densities ranging from 0.2-3.1×10^{19} m^{-3}. The neutral diffusivity coefficient (D_n) is set to just over 200 m^2/s everywhere; this value is lower than the neutral diffusivity estimated [15]. The lower D_n can be somewhat justified as lower divertor/target temperatures would be obtained if more physics, such as the missing atomic processes, would be included in the model, and at lower temperatures the neutral diffusivity is lower. "S Korving, GTA Huijsmans et al" are currently working on advanced SOL/divertor modelling, within JOREK, which can be used for future work.

Fig. 1.a) shows as the mid-plane separatrix density is increased there is a roll-over in the target parallel electron density flux to the outer target, indicating a high neutral density, cold divertor and detachment for the highest upstream density cases. As the roll-over occurs the electron temperature at the target decreases below 5 eV. The roll-over is not steep but the ionisation front, in Fig. 1.b), is also seen to move off of the target upstream as the roll-over occurs. A comparison has been made to SOLPS, for this JOREK MAST-U Super-X H-mode case (labelled R5 in Fig. 2.). The SOLPS results shown in Fig. 1.a) are from [10], where the MAST-U equilibrium with expanded flux is used. In JOREK the perpendicular diffusivity profiles were set to be the same as SOLPS. The comparison shows that the higher upstream density results from JOREK are not as deeply detached as SOLPS, due to the shallow roll-over observed. Divertor pumping was included, without pumping the divertor appeared to always be detached. A scan in pumping speed is given in [15]. The addition of the pumps modifies the densities and temperatures at the targets, while only slightly affecting the upstream profiles just outside the separatrix.

Also, in [15] a comparison between JOREK and SOLPS for an attached L-mode MAST case and a H-mode MAST-U Super-X case without expanded divertor flux is given. The MAST-U Super-X case without expanded flux given in [15] at a mid-plane plane separatrix density of 2.0×10^{19} m^{-3} is used for the ELM simulations in the following sections (labelled R4 in Fig. 2). This case is closest in terms of target parallel electron density flux in a comparison to SOLPS results from [10]. No divertor pumping is included in this case, however, MAST-U will have cryopumps in the Super-X divertor to remove impurities and for density control.

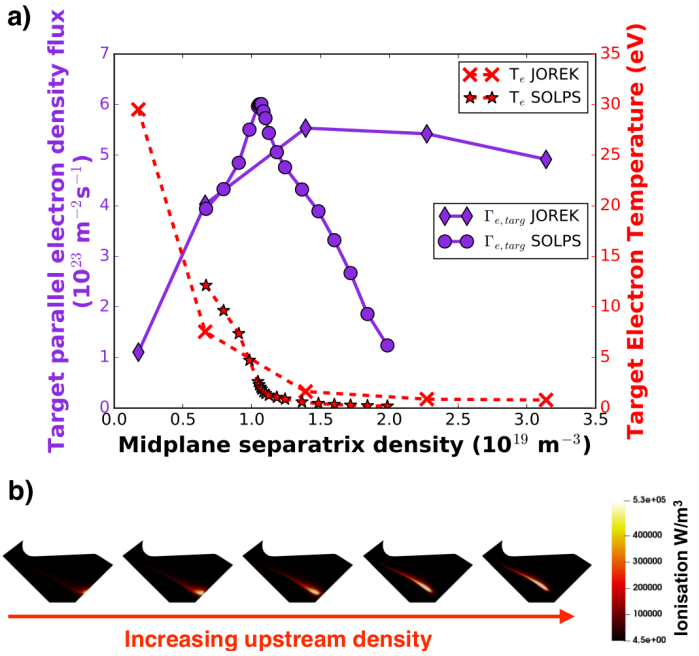

FIG. 1. (a) The target parallel electron density flux and target electron temperature as a function of upstream density, comparing JOREK with SOLPS [10]. (b) The ionisation front in the lower divertor, from the JOREK simulations.

4. ELM BURN-THROUGH SIMULATIONS

As mentioned a MAST-U Super-X case without expanded divertor flux has been used in the ELM burn-through simulations, where a multiple toroidal mode number simulation has been performed. Before the results from the multi-mode simulation are given in section 4.2, an investigation to the effect on ELM energy fluence is performed in section

4.1. The results in section 4.1, unless otherwise stated, were obtained using the visco-resistive MHD model in JOREK where T_i=T_e and neutrals are not included.

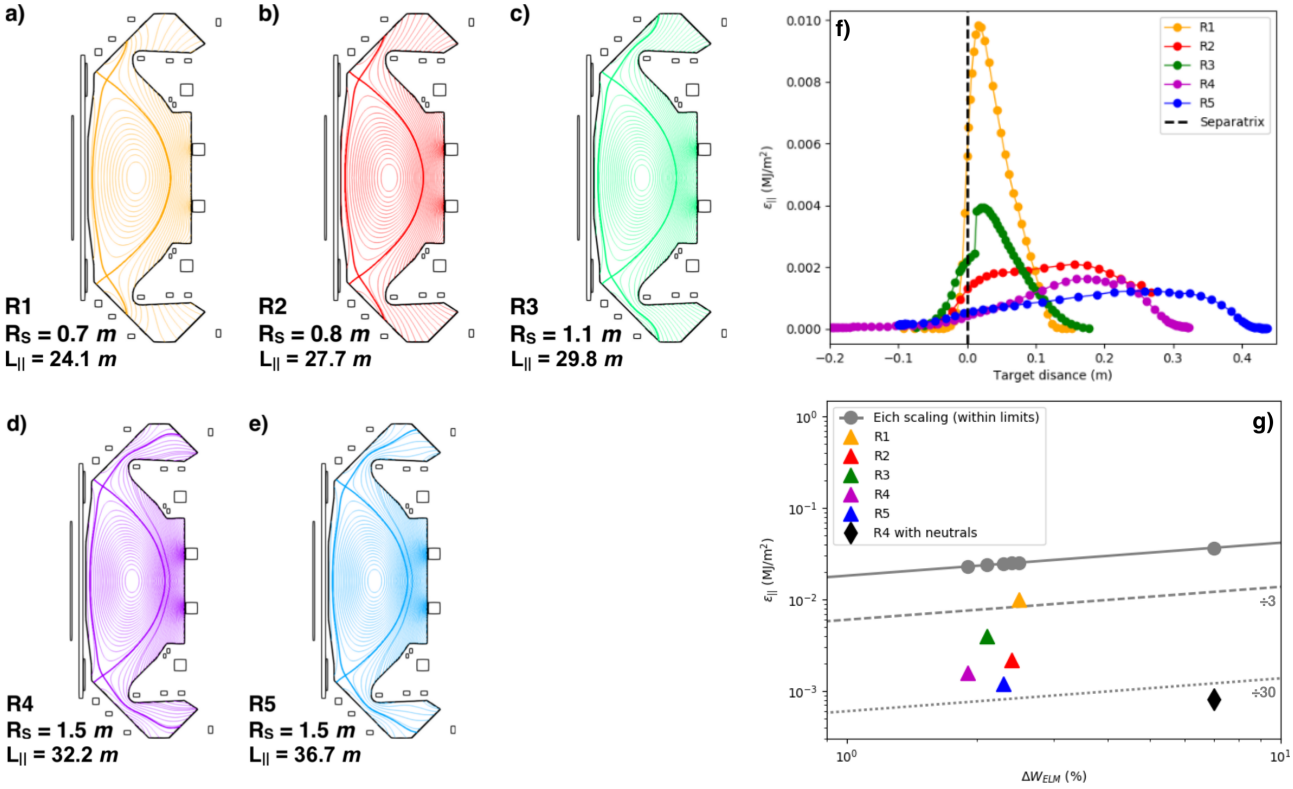

FIG. 2. Poloidal plane flux contour plots for a conventional MAST-U divertor (a) extending the outer leg (b) and (c) towards a Super-X divertor. The Super-X configuration (d) with no flux expansion in the divertor chambers and (e) with flux expansion. The black boxes indicate the coil positions and the thicker coloured lines show each separatrix. R_s is the strike point radius and $L_{||}$ is the connection length from mid-plane to target at Ψ_n =1.0001. (f) Profiles of the ELM energy fluence ($\varepsilon_{||}$) as a function of target distance for each of the divertor configurations. (g) The peak ELM parallel energy fluence as a function of ELM energy loss (note axes in log scale). $\varepsilon_{||}$ is given for Eich ELM scaling within regression limits given by grey circles. The coloured triangles represent the different divertor configuration simulations and the black diamond indicates the Super-X case run with the neutrals model.

4.1 ELM energy fluence comparison

A comparison of the ELM energy fluence for different divertor configurations is performed. The initial equilibria for each of the MAST-U cases have the same profiles, with the only difference being the outer leg length; each of the cases are given in Fig. 2.a) - e) where the flux contours are shown. Starting from a conventional case Fig. 2.a), where the strike point is at R_s = 0.7 m, to the Super-X case in Fig. 2.d) and a Super-X case with expanded flux, Fig. 2.e), which have strike points at R_s = 1.5 m. These cases may be referred to as R1-R5 represented by the different divertor configurations in Fig. 2.a) - e) respectively.

An ELM simulation is performed for each of the five cases with a single toroidal mode number (n=20). The instability growth rates are very similar for each of the cases as expected for the same equilibrium profiles; with a mean growth rate of 3.4×10^4 s^{-1} and standard deviation of 9.8×10^1 s^{-1}. The pedestal particle and energy losses due to the ELM are also very similar; the mean percentage pedestal particle loss is 12.8% with a standard deviation of 0.75%, the mean percentage energy pedestal loss is 10.4% with a standard deviation of 0.49%. The pedestal losses approximately correspond to 0.8 kJ and 1.1×10^{19} particles for each of the cases. The simulations show transitioning from a conventional case to the Super-X case reduces the peak heat fluxes by a factor 11 from 8 MW/m^2 to 0.7 MW/m^2. This can be understood by considering the area the heat flux is incident on - approximately 0.14 m^2 in the conventional case to 1.5 m^2 in the Super-X case. The comparison between R1 and R5 divertor configurations appears to be reasonable considering the change in target area. However, the peak heat fluxes are in general smaller than expected in comparison to target heat fluxes from ELMs in previous MAST experiments [23].

The parallel energy fluence ($\varepsilon_{||}$) is calculated for each of the divertor configurations. $\varepsilon_{||}$ is calculated by integrating the parallel heat flux ($q_{||}$) for the duration of the ELM, defined by Eich et al. [24] as

$$\varepsilon_{||}(s) = \int_{t_{\mathrm{ELM}}} \alpha_B q_{||}(s,t)\mathrm{d}t \qquad (1)$$

where α_B is the angle between the magnetic field lines and the divertor target and s is the distance along the target. Fig. 2.f) shows profiles of $\varepsilon_{||}$ as a function of the target distance for each of the divertor configurations, where the separatrix position is given by the black dashed line. $\varepsilon_{||}$ is largest for the conventional divertor configuration (R1) and is spread over a narrower target distance. R3 has a higher peak $\varepsilon_{||}$ than R2, however, it is seen $\varepsilon_{||}$ is spread further over the target, also note α_B is smaller for the R2 configuration. The peak $\varepsilon_{||}$ for the Super-X configurations, with (R5) and without (R4) expanded flux, are approximately a factor 8 and 6 lower than $\varepsilon_{||}$ for R1, respectively, and a spread along the target is observed. The empirical scaling of the ELM parallel energy fluence, obtained from experimental data analysis on multiple tokamaks in [24], is used for a comparison to the JOREK simulations for MAST-U. In [24] $\varepsilon_{||}$ is given as

$$\varepsilon_{||}(\mathrm{MJ/m^2}) = 0.28 \pm 0.14 \times n_{\mathrm{e,ped}}^{0.75\pm0.15} \times T_{\mathrm{e,ped}}^{0.98\pm0.1} \times \Delta W_{\mathrm{ELM}}^{0.52\pm0.16} \times R_{\mathrm{geo}}^{1.0\pm0.4} \qquad (2)$$

Fig. 2.g) shows $\varepsilon_{||}$ as a function of the ELM energy loss (ΔW_{ELM}). For the simulations performed ΔW_{ELM} is the only quantity in equation (2) which differs between the simulations. The grey solid line in Fig. 2.g) shows the Eich ELM scaling (within regression limits) and the grey circles indicate $\varepsilon_{||}$ as predicted by equation (2) for the cases R1-R5 and the Super-X R4 case with neutrals, using the value of ΔW_{ELM} from the simulation. The coloured triangles represent $\varepsilon_{||}$ calculated from the simulation results for the different divertor configurations. The conventional divertor configuration (R1 yellow triangle) is the case with the best agreement to the Eich ELM scale at less than a factor three from the estimate for the scaling law. Note, in [25] some of the JOREK JET cases, also without diamagnetic terms, are close to or just outside three times the estimate. The Super-X cases R4 (purple triangle) and R5 (blue triangle) appear to deviate from the empirical scaling, for these the parallel energy fluences are a factor 30 different compared to the exact Eich ELM scaling. The R4 and R5 cases show deviations of factors 14 and 22 respectively, from the scaling at the limit extents, comparing the purple and blue triangles to the solid grey line in Fig. 2.g). The peak $\varepsilon_{||}$ for the multiple toroidal mode number (R4) simulation with neutrals, which has a detached divertor before the ELM occurs (results of which will be given in the following subsection) is represented by the black diamond in Fig. 2.g). The peak $\varepsilon_{||}$ is lower for this case than the R4 case, using the single temperature model without neutrals (purple triangle), despite having over double the ELM energy loss. Here, $\varepsilon_{||}$ is a factor 46 lower than the Eich ELM scaling (within regression limits). The results indicate that not only do the extended leg cases deviate from the Eich ELM scale but also a detached plasma, before an ELM, causes an even larger deviation. The deviation is a promising result as $\varepsilon_{||}$ decreases, indicating the ELM could be somewhat buffered if the divertor is in a Super-X configuration and/or a detached regime.

4.2 Multiple toroidal mode number ELM simulation in the MAST-U Super-X configuration

A multi-mode number ELM simulation was performed with the JOREK diffusive neutrals, two temperature model. The extent of the plasma burn-through in the Super-X divertor during an ELM, is investigated. The multi-mode number ELM simulations are constrained by computational resources, so it has only been possible to simulate multiple toroidal mode numbers of n=2, 4, 6, ..., 20. The inclusion of multiple toroidal mode numbers (n) leads to a violent crash and more suppressed MHD activity after the ELM in comparison to a single mode number simulation, where the filamentary oscillations are long lived. For this simulation the MHD parameters are given in [15] and the reflectivity coefficient is set to 95%. The detached divertor state, mentioned in section 3, is used as a starting point for the ELM simulation. After a cold divertor has been obtained n=2, 4, 6, 8, 10, 12, 14, 16, 20 perturbations are added to the simulation, the energy of the mode numbers grow, shown in Fig. 3.a), and when the ELM crash occurs n=10 is the dominant mode number. The ELM crash leads to increased fluxes to the divertor and burn-through is observed in the Super-X. After the crash, recovery times can be calculated and a saturation phase with lower MHD activity occurs.

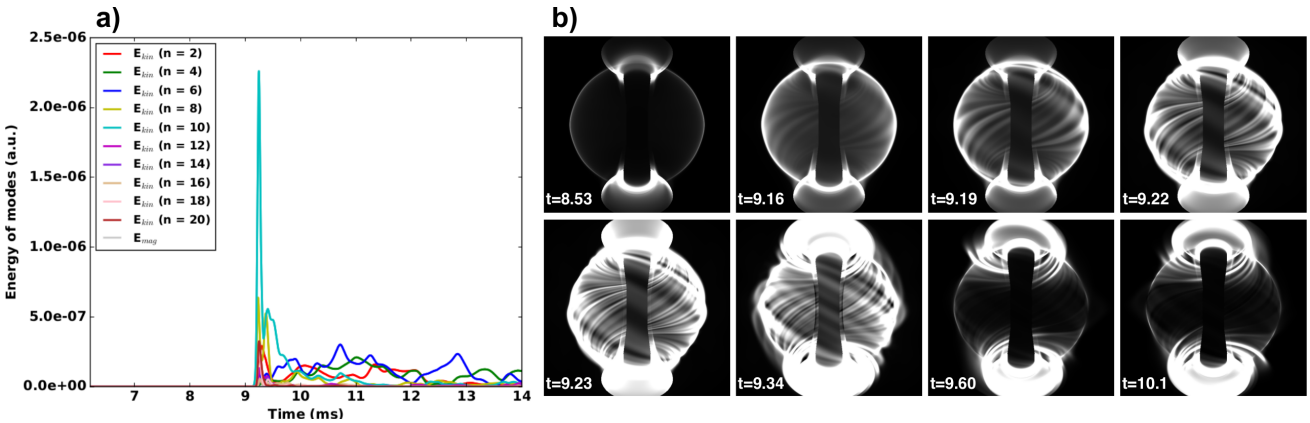

FIG. 3. (a) The evolution of the kinetic energy (coloured lines) of the mode numbers for the multi-mode simulation. (b) The evolution of the filamentary structures during the multi-mode ELM simulation imaged with a synthetic fast camera diagnostic (time given in ms).

The evolution of the non-linear structure of the ELM filaments is observed using the JOREK synthetic fast camera diagnostic, Fig. 3.b). The JOREK fast camera diagnostic code was developed and first used for MAST simulations shown in [14]. This code has now been slightly adapted as the neutral density can be used directly from the simulation data instead of applying a fit, which was previously done. Per image there are 384,000 pixels corresponding to the lines of sight on which the radiation is integrated over, where the photon emissivity coefficient data is given as a function of density and temperature, using ADAS data. The examples of the JOREK fast camera during the simulation, given in Fig. 3.b), start from a well-confined plasma before the instability occurs (top-left). Filaments then start to form and violently erupt into the scrape-off-layer and start to rotate. The non-linearity of the ELM filaments due to mode interaction is apparent, in comparison to the more uniform filament structure of the single mode number simulations, given in [15]. When the crash occurs an increase in the visible light is then seen in the divertor regions, due to the flux of heat and particles. The visible light in the divertor region is so bright that a filter had to be applied to the synthetic diagnostic, restricting the maximum light, in order to observe the filaments. After the ELM crash, the filaments start to reduce in size, whilst the divertor remains bright (two lower-right images of Fig. 3.b)).

In the simulation the violent crash leads to a quick burn-through, where the pedestal thermal energy loss is 1400 J, during the ELM. A simple analytical calculation is performed to determine the extent of the ELM burn-though given the neutral density in the Super-X chamber before the ELM. The neutral density in the lower divertor has been integrated over the volume of the Super-X chamber to determine the number of neutral particles. This is calculated to be 2.9×10^{18} particles, the ionisation energy per neutral particle is 13.6 eV. Therefore, it would take 6.5 J for all the neutrals in the lower divertor to be ionised. Assuming all the energy lost from the pedestal, during the ELM crash, goes to the divertor regions then 1050 J would go to the lower divertor, taking the same up-down ratio of the heat fluxes. This simple calculation indicates ELM burn-through will occur unless the ELM size is a factor 160 lower or there is a factor 160 more neutrals in the lower divertor for the ELM to be completely buffered. However, the ELM is partially buffered with the inclusion of neutral particles in the simulations, not only is energy taken from the ELM to ionise the neutral particle front in the divertor but as the density flux from the ELM arrives on the target, even more neutrals are being reflected from the wall, and these neutrals also need to be ionised by the ELM energy before it is incident on the target.

The evolution of the peak outer lower target values, of the heat flux, plasma density, electron temperature, and neutral density, are give in Fig. 4.a). The peak heat flux to the outer lower target, due to the ELM, is 9.8 MW/m^2 and is a factor three lower to the upper outer target. The peak heat flux arrives roughly 0.1 ms after the ELM crash, and 1.5 ms after the crash the heat flux has relaxed to almost pre-ELM conditions. The heat flux pattern, given in Fig. 4.b), shows at the start the peak heat flux is located just outside the separatrix (white dashed line). The peak in heat flux then rapidly, in around 0.1 ms, moves along the outer target to around 20 cm from the separatrix, before it travels back towards the separatrix with a significantly reduced amplitude. The peak electron temperature on the upper and lower outer targets is 150 eV and recovers to below 5 eV, almost pre-ELM conditions, around 3 ms after the crash, shown in Fig. 4.a). In the simulation before the ELM there is a higher plasma and neutral density and lower electron temperature in the lower divertor in comparison to the upper divertor. During the ELM crash the filaments rotate due to the intrinsic E×B rotation caused by the ELM itself. This rotation leads to a non-symmetric distribution of fluxes to the upper and lower divertors. The simulation results show that more plasma density is diverted to the lower divertor during the ELM than the upper divertor (Fig. 4.a) and 5.a)); because of this there is a larger burn-through observed in the lower divertor and a higher peak heat flux, which is roughly three times more, in the lower divertor (Fig. 4.a)). Consequently, a higher neutral density is observed in the lower divertor, in comparison to the upper divertor, just after the ELM. The peak target electron temperatures, due to the ELM, are the same in both divertors and the recovery time to almost pre-ELM conditions is the same. The heat flux recovery times are similar in both divertors (Fig. 4.a)).

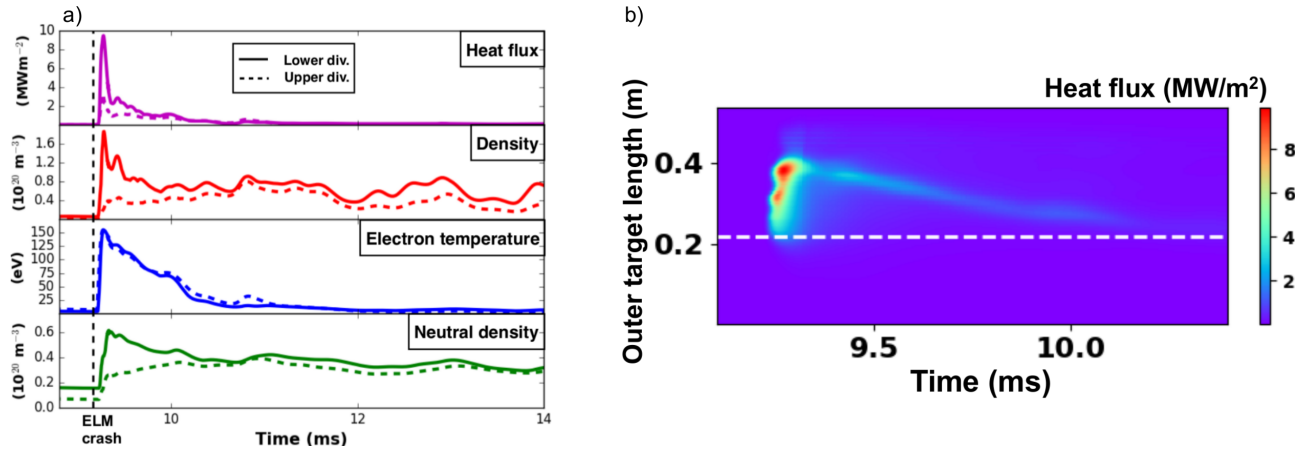

FIG. 4. (a) The evolution of the peak outer target values for the heat flux, density, electron temperature and neutral density for the upper (dashed lines) and lower (solid lines) divertors. (b) The heat flux pattern onto the Super-X lower outer target during the ELM simulation, zoomed in time to the peak heat flux to the target, from the ELM crash. White dashed line is the separatrix position.

The density and electron temperature, in the poloidal plane, during the ELM are given in Fig. 5.a) and b) respectively. The density filaments extend further into the SOL and finger-like structures are observed around the X-point and in the divertor region; this is also seen in the electron temperature. Due to the higher density and temperature around the baffle region the peak heat flux onto the baffle is calculated. The peak heat flux is 2 MW/m^2 to the baffle, a factor of 5 lower than the peak heat flux to the outer target of the Super-X. Due to the baffle position it could be an issue during large ELMs; however, the baffle in MAST-U has been covered with carbon tiles to manage this. The magnetic field structure is plotted to observe whether the finger-like structures are due to the magnetic field. The Poincaré plot in Fig. 5.c) shows the whole region around the strike point is ergodised, with field lines connecting the pedestal top to the target.

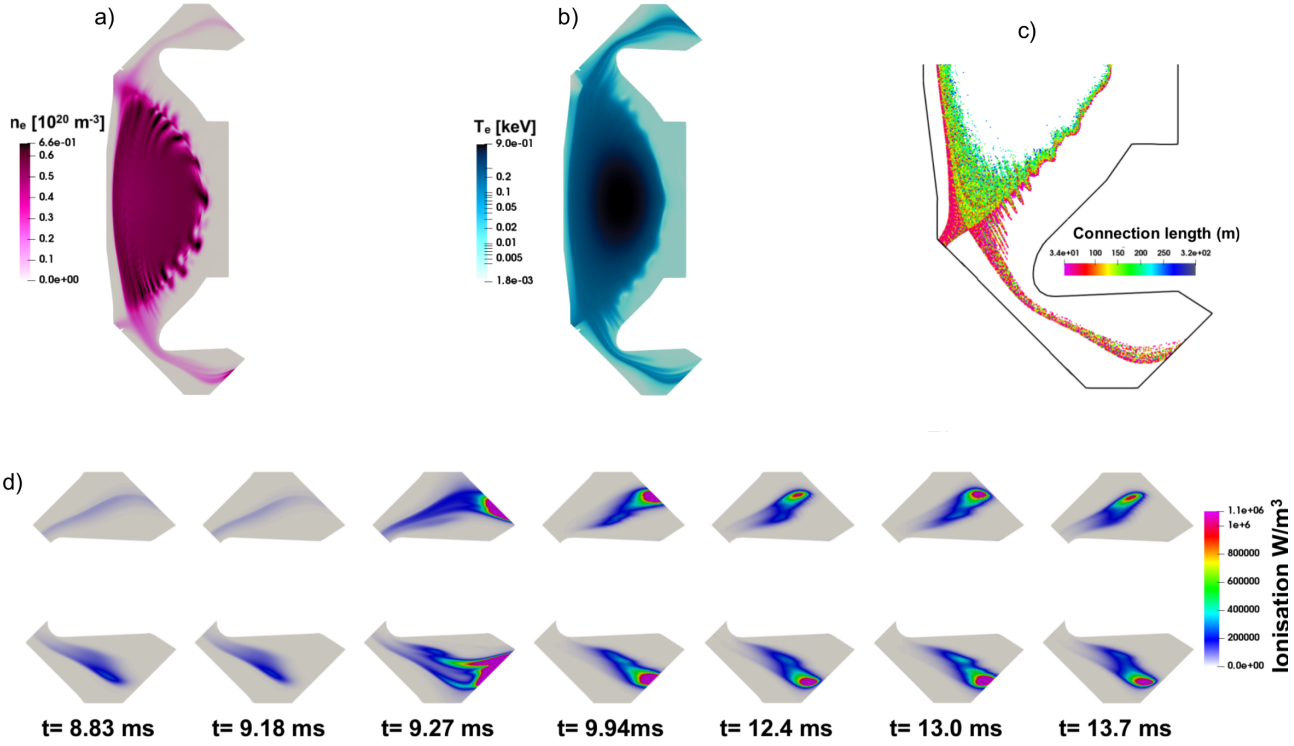

FIG. 5. Poloidal plots of the density (a) and electron temperature (b) during the ELM. (c) Poincaré plot of the magnetic field structure during the ELM. (d) The evolution of the ionisation fronts in the upper and lower outer Super-X divertors during the ELM simulation.

The evolution of the ionisation in the lower outer Super-X divertor, during the ELM simulation, is shown in Fig. 5.d). Starting from a detached divertor before the ELM at t = 8.83 ms, as the ELM crash starts at approximately t = 9.18 ms the ionisation front is still upstream and the divertor is still detached. At approximately t = 9.27 ms the peak heat flux is incident on the outer divertor targets and the ionisation has significantly increased on and in front of the outer targets. 2 ms after the crash the ionisation front is still at the target and the electron temperature is above 10 eV for both divertors so it is assumed the plasma is still attached at this point of the simulation. The ionisation decreases 1 ms after the ELM crash and at 12.4 ms the plasma starts to detach in both the upper and lower divertors, the peak electron target temperature has decreased to below 5 eV and the ionisation front starts to move off the target, indicating the plasma may detach again after the ELM, during the inter-ELM phase. The detached regime is not long lived in the lower divertor due to the MHD activity of the lower toroidal mode numbers and the lower divertor attaches again. At around 13.7 ms the lower divertor appears to detach as the peak target temperature drops again below 5 eV and the ionisation front moves upstream. The upper divertor remains detached after 12.4 ms but by analysing the ionisation in the divertor it appears that the divertor is not deeply detached after the ELM crash.

5. SUMMARY

ELM simulations for the MAST-U Super-X configuration have been explored. The single temperature visco-resistive reduced MHD simulations without neutrals indicate there is a factor 11 reduction in the peak heat flux to the outer target of the Super-X in comparison to a conventional divertor configuration. The ELM energy fluence for MAST-U has been investigated. The conventional divertor case shows agreement of $\varepsilon_{||}$ to the Eich ELM scaling law but the Super-X extended leg configurations differ. However, whilst $\varepsilon_{||}$ deviates from the scaling, it is significantly lower for the Super-X cases. The results suggest the scaling may have to be adapted for extended leg divertors and for detached plasmas, but are promising as they indicate Super-X detached plasmas will have decreased ELM energy fluences. A roll-over in the target parallel electron density flux for a MAST-U H-mode case is obtained. As the divertor detaches the target electron temperature drops below 5 eV and the ionisation front moves upstream. A detached case after the roll-over is used as a starting point for the ELM burn-through simulation.

An ELM burn-through simulation has been obtained with the neutrals model. It is seen that n=10 is the dominant mode number. The multi-mode number simulation performed gives a peak ELM heat flux of ~9.5 MW/m^2 at the lower Super-X target. The plasma appears to detach around 3 ms after the ELM, however, in the lower divertor the plasma is not as deeply detached as before the ELM, due to the MHD activity after the ELM.

When the first physics campaign for MAST-U starts in the near future, questions about the behaviour during ELMy H-mode in the Super-X configuration can be answered, until then the simulations presented here can provide useful guidance. The ELM simulations with the neutrals model show the plasma burn-through the neutrals front in the Super-X divertor. Recovery times to pre-ELM conditions in the divertor are on the order of a few milliseconds in each case where the neutral density in the divertor is high enough. The recovery times are shorter than the inter-ELM phase for large ELMs in previous MAST experiments; indicating promising results with regards to future experiments on the MAST-U Super-X tokamak.

ACKNOWLEDGEMENTS

This work has been carried out within the framework of the EUROfusion Consortium and has received funding from the Euratom research and training programme 2014-2018 and 2019-2020 under Grant Agreement No. 633053 and from the RCUK Energy Programme (Grant No. EP/P012450/1) as well as the Fusion CDT Programme through the EPSRC (Grant No. EP/L01663X/1). The views and opinions expressed herein do not necessarily reflect those of the European Commission. This work used the MARCONI computer at CINECA and the PRACE MareNostrum computer under project Tier-0 JVSITPEI.

REFERENCES

[1] Wagner F. et al 1982 Regime of Improved Confinement and High Beta in Neutral-Beam-Heated Divertor Discharges of the ASDEX Tokamak Phys. Rev. Lett. **49** 1408–12
[2] Leonard A.W. 2014 Edge-localized-modes in tokamaks Phys. Plasmas **21** 090501
[3] Kirk A. et al 2012 Observation of Lobes near the X Point in Resonant Magnetic Perturbation Experiments on MAST Phys. Rev. Lett. **108** 255003
[4] Lang P.T. et al 2014 ELM pacing and high-density operation using pellet injection in the ASDEX Upgrade all-metal-wall tokamak Nucl. Fusion **54** 083009
[5] de la Luna E. et al 2016 Understanding the physics of ELM pacing via vertical kicks in JET in view of ITER Nucl. Fusion **56** 026001
[6] Fishpool G. et al 2013 MAST-upgrade divertor facility and assessing performance of long-legged divertors J. Nucl. Mater. **438** S356–9
[7] Katramados I. et al 2011 MAST upgrade closed pumped divertor design and analysis Fusion Eng. Des. **86** 1595–8
[8] Kukushkin A.S. et al 2015 Characteristics of divertor detachment for ITER conditions J. Nucl. Mater. **463** 586–90
[9] Havlickova E. et al 2015 SOLPS analysis of the MAST-U divertor with the effect of heating power and pumping on the access to detachment in the Super-x configuration Plasma Phys. Control. Fusion **57** 115001
[10] Moulton D., Lipschultz B. and Harrison J. 2017 Detachment onset in MAST-U according to SOLPS-ITER 44th EPS Conf. Plasma Physics (Belfast, United Kingdom, 26–30 June 2017) O5.129 (http://ocs.ciemat.es/EPS2017PAP/pdf/O5.129.pdf)
[11] Huysmans G.T.A. and Czarny O. 2007 MHD stability in X-point geometry: simulation of ELMs Nucl. Fusion **47** 659–66
[12] Czarny O. and Huysmans G. 2008 BÅLezier surfaces and finite elements for MHD simulations J. Comput. Phys. **227** 7423–45
[13] M Hoelzl, GTA Huijsmans, SJP Pamela, M Becoulet, E Nardon, FJ Artola, B Nkonga, et al The JOREK non-linear extended MHD code and applications to large-scale instabilities and their control in magnetically confined fusion plasmas Nuclear Fusion (submitted); preprint at: arXiv:2011.09120
[14] Pamela S.J.P. et al 2013 Resistive MHD simulation of edge-localized-modes for double-null discharges in the MAST device Plasma Phys. Control. Fusion **55** 095001
[15] S.F. Smith et al Nucl. Fusion **60** (2020) 066021
[16] Fil A. et al 2015 Three-dimensional non-linear magnetohydrodynamic modeling of massive gas injection triggered disruptions in JET Phys. Plasmas **22** 062509
[17] Summers H.P. Atomic Data and Analysis Structure User Manual www.adas.ac.uk/
[18] Siobhan Smith. Numerical simulations of edge localised mode instabilities in the MAST-U Super-X tokamak. PhD thesis, University of York, sep 2019. URL http://etheses.whiterose.ac.uk/26275/.
[19] Cunningham G. 2013 High performance plasma vertical position control system for upgraded MAST Fusion Eng. Des. **88** 3238–47
[20] Pangione L., McArdle G. and Storrs J. 2013 New magnetic real time shape control for MAST Fusion Eng. Des. **88** 1087–90
[21] Pamela S., Huijsmans G., Thornton A.J., Kirk A., Smith S.F., Hoelzl M. and Eich T. 2019 A wall-aligned grid generator for non-linear simulations of MHD instabilities in tokamak plasmas Comput. Phys. Commun. **243** 41–50
[22] Xavier B., Wouter D., Richard P., David C., Serguey V. and Sven W. 2016 Presentation of the New SOLPS-ITER Code Package for Tokamak Plasma Edge Modelling Plasma Fusion Res. **11** 1403102–1403102
[23] Thornton A.J., Kirk A., Chapman I.T. and Harrison J.R. 2013 Divertor heat fluxes and profiles during mitigated and unmitigated edge localised modes (ELMs) on the Mega Amp Spherical Tokamak (MAST) J. Nucl. Mater. **438** S199–202
[24] Eich T., Sieglin B., Thornton A.J., Faitsch M., Kirk A., Herrmann A. and Suttrop W. 2017 ELM divertor peak energy fluence scaling to ITER with data from JET, MAST and ASDEX upgrade Nucl. Mater. Energy **12** 84–90
[25] Pamela S.J.P. et al 2017 Recent progress in the quantitative validation of JOREK simulations of ELMs in JET Nucl. Fusion **57** 076006 7